MECHANICAL PROPERTIES, PHYSICS
OF STRENGTH, AND PLASTICITY

Microplasticity of Amorphous and Crystallized Fe$_{78}$P$_{20}$Si$_2$ Alloy

V. M. Ievlev[a, b], **S. V. Kannykin**[b,]*, **T. N. Il'inova**[c], **V. V. Vavilova**[d],
D. V. Serikov[e], **and A. S. Baikin**[d]

[a]*Moscow State University, Moscow, 119991 Russia*
[b]*Voronezh State University, Voronezh, 394036 Russia*
[c]*Burdenko State Medical University, Voronezh, 394036 Russia*
[d]*Baikov Institute of Metallurgy and Materials Science, Russian Academy of Sciences, Moscow, 119334 Russia*
[e]*Voronezh State Technical University, Voronezh, 394006 Russia*
***e-mail: svkannykin@gmail.com**
Received December 18, 2018; revised March 6, 2019; accepted March 12, 2019

Abstract—In order to determine the mechanism of plastic deformation, the hardness and local plasticity of amorphous Fe$_{78}$P$_{20}$Si$_2$ alloy are compared at different stages of its crystallization activated by thermal treatment at 300–750°C or short-term photon treatment with a radiation dose coming to the sample of 10–60 J/cm^2. The phase composition and structure were investigated by X-ray diffractometry and high-resolution transmission electron microscopy. With the same sequence of structural changes, the crystallization rate under photon treatment is more than two orders of magnitude higher than that under thermal treatment, which indicates the effect of a high rate of input of the process activation energy. The nonmonotonic dependence of the hardness, elastic modulus, and the proportion of plastic strain in the indentation work is found, depending on the annealing temperature or radiation dose received by the sample, as a result of structural changes in the alloy. The local plasticity of the initial alloy and fully crystallized alloy are close in magnitude. Based on the features of the crystal structure of the Fe$_3$P phase (the impossibility of the dislocation mechanism of plastic deformation) and assuming that the structural unit (tetrahedral Fe$_3$P cluster) of the crystallized and amorphous alloy is identical, a conclusion was formulated about the cluster mechanism of plastic deformation of the amorphous alloy.

1. INTRODUCTION

The limited experimental data on the local atomic structure, the absence of translational symmetry, and the inapplicability of ideas about the types of defects inherent in crystalline materials leave the nature of the plasticity of amorphous alloys (AAs) unresolved. At present, there is a generally accepted view that the elementary process underlying the deformation in amorphous alloys consists of the local rearrangement of low-atomic clusters that take on shear stress [1]. An example of such a local rearrangement was first proposed in [2] based on the atomic-analog bubble model. It was called the "fluidity defect" or "τ defect" [3], and recently the term "shear transformation zone" (STZ) [4] has been used. A shear transformation zone is a local group of atoms that undergo a shear change in the configuration of relatively low energy into a second similar configuration. An alternative interpretation of the mechanism of plasticity in amorphous alloys is given in the framework of the conventional "free volume" model as it was developed [5] and applied in considering the deformation of metallic glasses [6]. Both approaches are essentially phenomenological and do not take into account the features of the real structure of amorphous alloys.

We cannot exclude intercluster slippage (an analogue of intergranular slippage in nanocrystalline materials) as one of the possible mechanisms for the manifestation of microplasticity of amorphous alloys and a large fraction of plastic deformation in the nanoindentation deformation work.

The idea of the cluster mechanism of deformation of amorphous alloys is not new; it is presented in [7] without specifying materials and corresponding low-atom clusters. The cluster organization of the structure of silicate glass has been discussed for several decades and is now considered proven [8].[1] The organization of the metal–metalloid structure of amorphous alloys, based on the cluster model, was studied by the molecular dynamics method using the Fe–B and Fe–P systems [10]. The commonality of the char-

---

[1] Within the scope of the article, it should be noted that both fused quartz and sodium silicate glass have a significant proportion of the plastic component in the nanoindentation deformation work [9].
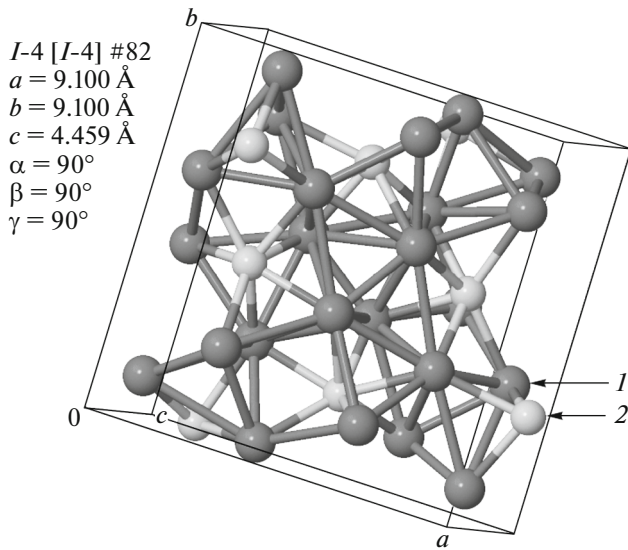
I-4 [*I*-4] #82
a = 9.100 Å
b = 9.100 Å
c = 4.459 Å
α = 90°
β = 90°
γ = 90°

Fig. 1. Unit cell of the Fe_3P phase: (*1*) Fe, (*2*) P [13].

acteristic structural units of crystalline hydroxyapatite and amorphous calcium phosphate of the same composition, with the impossibility of the dislocation mechanism of plastic deformation of crystalline hydroxyapatite, was used to substantiate the large magnitude of microplasticity in the crystalline and amorphous state [11] with their strongly pronounced brittleness, as well as structural transformations under conditions of comprehensive reduction of the microcrystalline sample [12].[2]

The purpose of this study is to compare the local plasticity of the amorphous and crystallized alloys of composition $Fe_{78}P_{20}Si_2$ in the assumption of the cluster organization of the amorphous alloy and on the basis of the structural organization of the Fe_3P crystalline compound.

We selected the $Fe_{78}P_{20}Si_2$ alloy because it is possible, according to the state diagram of the Fe−P system, to obtain a Fe_3P crystalline phase with the atomic structure shown in Fig. 1 [13] as the main phase (up to 80 vol %) after crystallization. Such a low translational symmetry of the crystal lattice eliminates the possibility of the dislocation mechanism of plastic deformation of crystalline Fe_3P.

Based on the features of the structure of the Fe_3P crystalline phase, it can be assumed that the main structural unit in the amorphous alloy of the corresponding composition, as energetically favorable, is the same. It is characterized by the tetrahedral structural unit corresponding to the compound chemical formula. An elementary cell of thirty-two atoms

---

[2] Weak translational symmetry of crystalline hydroxyapatite eliminates the formation of dislocations of deformation origin.

accounts for eight such units, and they are mutually disoriented within it.

2. EXPERIMENTAL

The amorphous alloy (Fe, 78 at %; P, 20 at %; and Si, 2 at %) was obtained by quenching from a liquid state in the form of tapes 3 mm wide and ~40 μm thick.

Samples were thermally treated under a vacuum of 10^{-3} Pa in the Anton Paar HTK-1200N chamber at 300, 350, 400, 550, 650, and 750°C for 10 min at each temperature; the heating rate was 10°C/min. After processing, the samples cooled with the chamber to room temperature.

The crystallization temperature during thermal treatment at a given heating rate was evaluated by differential scanning calorimetry (DSC). Based on the dependence of the crystallization rate on temperature, it was advisable to compare the effect of fast photon treatment in the crystallization of the amorphous alloy. Photon treatment was carried out in a vacuum of 10^{-3} Pa under the radiation of INP 16-250A pulsed xenon lamps (λ = 0.2−1.2 μm) at a dose (*D*) of radiation received by the sample of 10, 15, 20, 25, 30, 35, 40, and 60 J/cm² (the treatment time corresponding to these doses is 0.5, 0.75, 1, 1.25, 1.5, 1.75, 2, and 3 s) using an UOL.P-1M instrument.

Phase and structural transformations were studied by X-ray diffractometry (XRD) using an ARL X'TRA instrument (Thermo Scientific) in the geometry of a parallel beam; the optical circuit of a parabolic mirror−thin-film collimator was used. The recording was performed in the θ−θ mode; the samples were placed on silicon substrates with a "zero background." An X-ray tube with a copper anode (CuK_α) was used as a source, and inelastically scattered radiation was discriminated by a 250 eV semiconductor energy dispersive detector with a Peltier cooler. The proportion of the crystalline phase was estimated by the Huang method [14] from the equation

$$V_{cr} = I_{cr}(I_{cr} + \alpha I_a)^{-1},$$

where I_{cr} and I_a are the integrated intensities of reflections from the crystalline and amorphous phases, respectively, and α is a constant (the Huang parameter), which is close to unity for iron-based alloys [15]. The calculation was performed in the Crystallinity program, which is part of the WinXRD-2.05 software package. Ultrathin sections prepared using a Quanta 3D apparatus were studied by TEM with the use of an FEI Titan 80-300 instrument.

The local plasticity of the samples was evaluated by dynamic nanoindentation using a NanoHardness-Tester instrument (CSM Instruments). In nanoindentation, linear loading and unloading of the indenter was used; loading rate was 0.02 N/min, holding at maximum load was 1 s, and the unloading rate was 0.03 N/min. The indentation was performed with a
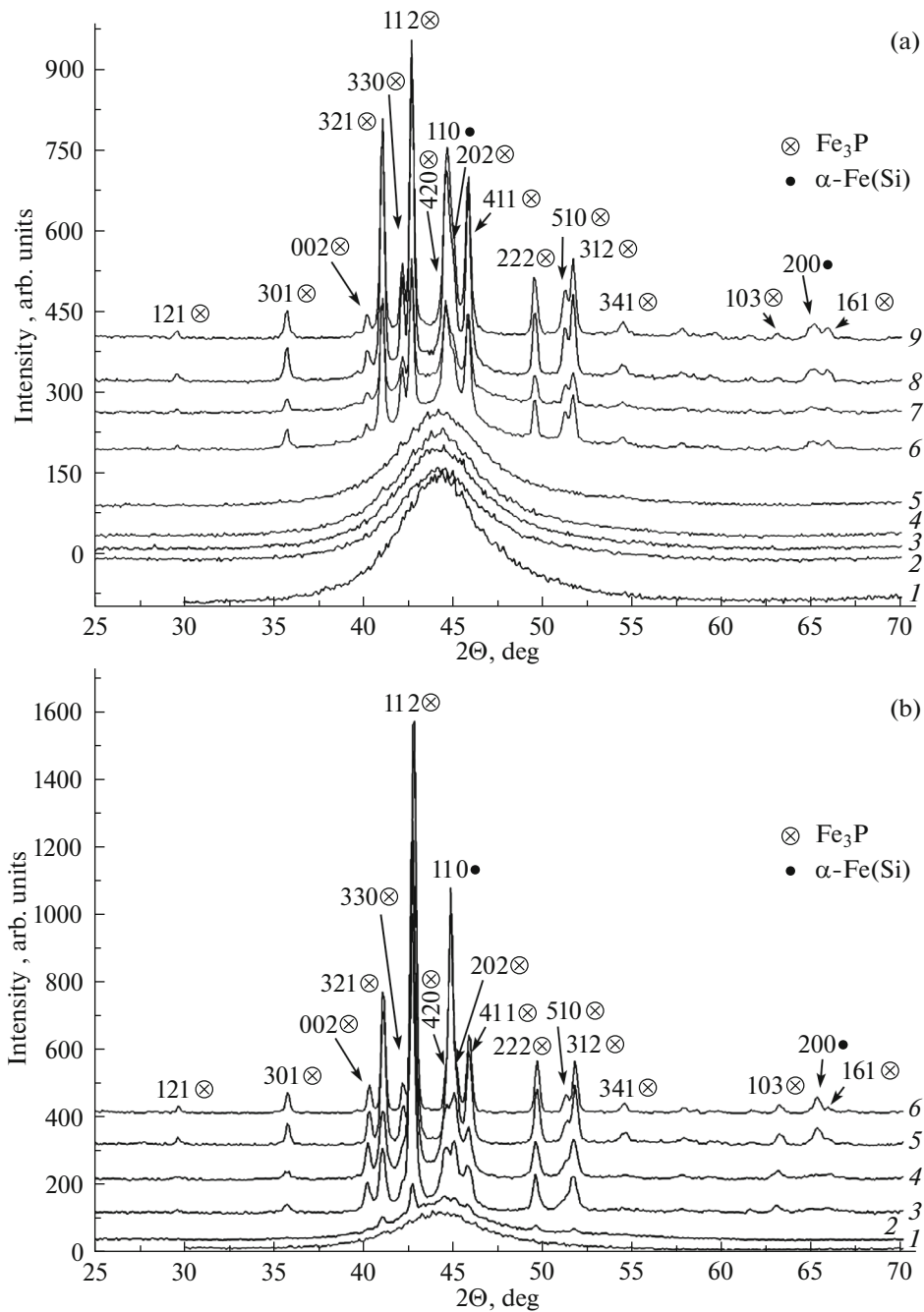
Fig. 2. X-ray diffraction patterns of amorphous alloy (a) (*1*) original and after thermal treatment at T = (*2*) 300, (*3*) 350, (*4*) 400, (*5*) 650, and (*6*) 750°C for 10 min and (b) (*1*) original and after photon treatment at a dose of radiation received by the sample of D = (*2*) 10, (*3*) 15, (*4*) 20, (*5*) 25, (*6*) 30, (*7*) 35, (*8*) 40, and (*9*) 60 J/cm^2.

maximum load on the indenter (*P*) of 30 mN. The Meyer hardness, elastic modulus, and the proportion of plastic deformation in indentation work were determined by the method of Oliver and Pharr [16]. For each load, the average values of these parameters were determined from the results of at least twenty measurements. Earlier [17], we found that at a load of 30 mN, the crystallization of the amorphous alloy under study does not occur in the indentation zone.

3. RESULTS AND DISCUSSION

3.1. Crystallization

X-ray diffraction patterns (Fig. 2) characterize the initial atomic structure and the change in the phase composition of the alloy at successive stages of (a) thermal and (b) photon treatment. The original structure is amorphous. The high-resolution TEM image of the cross section of the sample and the microelec-
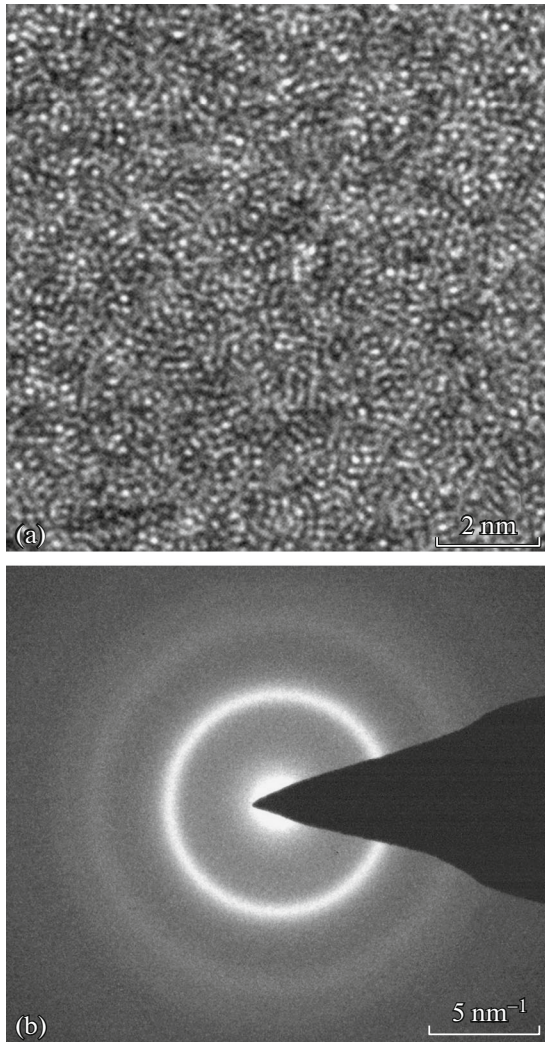
Fig. 3. (a) High-resolution TEM image and (b) microelectron diffraction pattern of the original amorphous alloy.

Fig. 4. DSC curves of heating the original amorphous alloy at a rate of (*1*) 5, (*2*) 10, (*3*) 20, and (*4*) 40°C/min.

tron diffraction pattern are shown in Fig. 3. The position of the maximum of the first halo in the electron diffraction pattern and in the X-ray diffraction pattern for the amorphous phase corresponds within the error to the position of reflections 110 of the solid solution of α-Fe and reflection 420 of crystalline Fe_3P. The features of the cluster organization of the structure of the amorphous alloy also affect the observed contrast of the high-resolution image.

The onset of crystallization corresponds to the DSC results for the heating mode used (10°C/min, Fig. 4). In this mode of annealing, the crystallization of the amorphous alloy begins with the separation of the main crystalline phase (a clear manifestation of reflections 112 and 321 of Fe_3P starting at $T = 300$°C). With increasing temperature, a solid solution of α-Fe(Si) is also formed. The crystallization is almost entirely completed at 600°C.

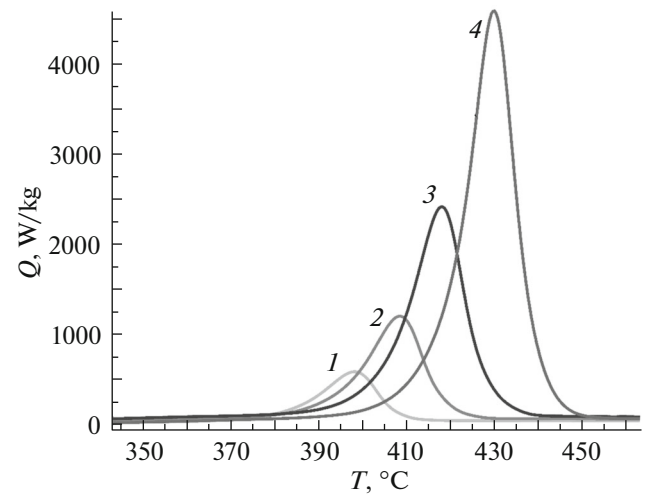Figure 2b shows X-ray diffraction patterns characterizing the crystallization of the amorphous alloy under photon treatment. The crystallization begins at $D = 30$ J/cm² and is completed at $D = 60$ J/cm². It follows from the comparison of Figs. 2a and 2b that the qualitative phase composition obtained as a result of the photon treatment is the same obtained by the thermal treatment. Taking into account the corresponding radiation dose received by the sample at the duration of the photon treatment of 0.5–4 s, the rate of the crystallization process is, on average, 200 times greater than that under thermal treatment.

The TEM image (Fig. 5a) characterizes the grain structure of samples crystallized under thermal treatment: the grain size of the Fe_3P phase and the solid solution phase are of a submicrometer scale (from 10 to 100 nm). The microelectron diffraction pattern (Fig. 5b) of the image region contains reflections corresponding to both phases; the precipitations of small solid solution particles within large grains is well revealed in high-resolution images (Fig. 5c) with reflection 110 of α-Fe(Si) (highlighted by hatching).

A significantly higher amplitude of atomic scattering of electrons compared to X-rays enables observing diffraction on the planes of the most significant period (the (110) planes of Fe_3P (Fig. 5b, highlighted due to the extremely weak contrast), despite the fact that their X-ray intensity is only 0.001 from the maximum (100 for planes (321)) and, accordingly, forming a periodic contrast in the high-resolution TEM image (Fig. 6) within the Fe_3P grains for the existing reflections 110 and their multiples (220 and 330, Fig. 6).

Under the conditions of different active reflections, no dislocations were revealed, which confirms the initial assumption based on the features of the
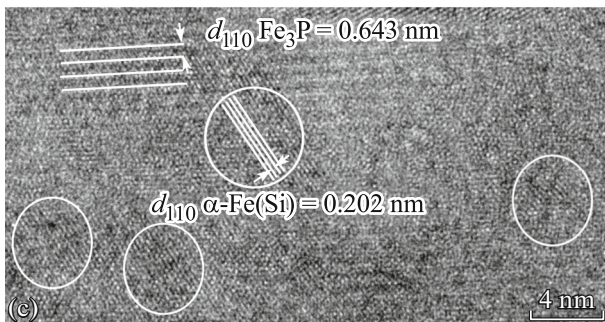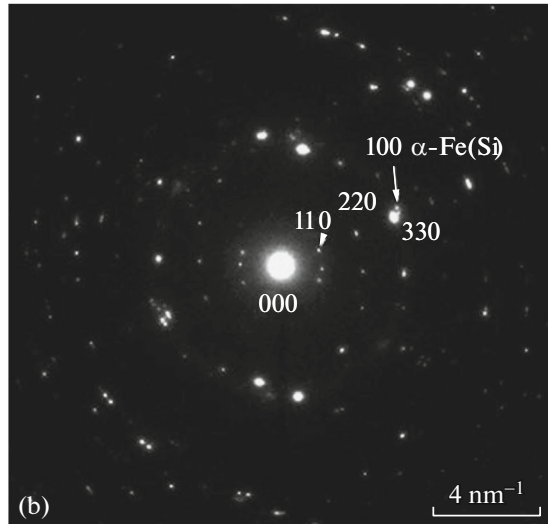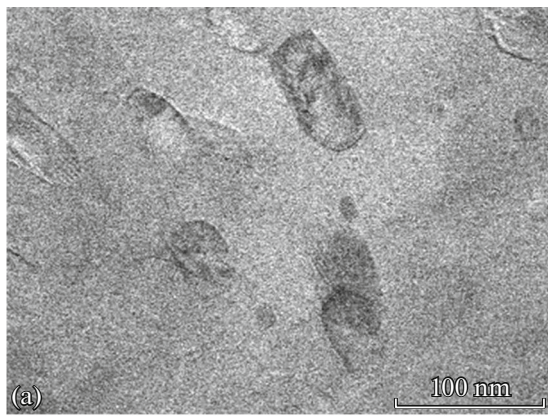
Fig. 6. High-resolution TEM image of the sample after thermal treatment at $T = 650°C$.

Fig. 5. (a) TEM image, (b) microelectron diffraction pattern, and (c) high-resolution TEM image in reflection (110) of α-Fe(Si) of the sample after thermal treatment at $T = 650°C$.

atomic structure of the crystal that the dislocations of deformation origin cannot exist in Fe_3P crystals.

3.2. Mechanical Properties

It is determined from the diagrams of load (P)—depth of penetration of the indenter (h) that the deformation of the initial and crystallized amorphous alloys at different modes of thermal and photon treatments is
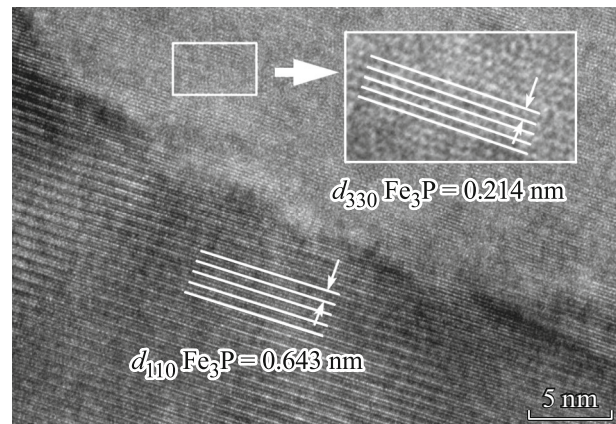
of an elastoplastic nature (Figs. 7 and 8). The hardness and modulus of elasticity of the original alloy are 8 ± 0.5 and 130 ± 5 GPa, respectively. A nonmonotonic change in the value of H (Figs. 9 and 10) with increasing dose or temperature generally has the same character and reflects the sequence of structural transformations activated by the photon or thermal treatment. The change in the modulus of elasticity is a consequence of the compositional nature of the structure. A large proportion (about 60%) of plastic deformation in the nanoindentation work is maintained up to 300°C at the thermal treatment and up to 15 J/cm^2 at the photon treatment with a slight decrease as a result of the completion of the structure relaxation stage of the amorphous phase.

The nucleation of crystalline phases leads to an increase in hardness and Young's modulus and a decrease in the proportion of plastic deformation in the nanoindentation process. At $T = 350°C$, the hardness was 11.4 ± 0.5 GPa, and Young's modulus was 137 ± 5 GPa with a plastic deformation fraction of 54%. With an increase in the annealing temperature to 400°C, the hardness and modulus of elasticity increased to 12.1 ± 0.5 and 161 ± 5 GPa, respectively, with a plastic deformation fraction of 52%. The maximum values of hardness and modulus of elasticity are 12.3 ± 0.5 and 164 ± 5 GPa with a plasticity fraction in the deformation work of 50%, and 11.4 ± 0.5 and 163 ± 5 GPa with a plasticity fraction of 50% at the thermal treatment at $T = 550°C$ and the photon treatment at $D = 35$ J/cm^2, respectively. For both types of treatment, the maximum hardness is recorded for the composite structure with a high concentration of nanocrystalline intermetallic compounds (their fraction is ~80%), which limits the plastic deformation of the amorphous phase. A further increase in temperature or dose leads to a decrease in hardness and an increase in the fraction of plastic deformation practically to the values of the original amorphous alloy.
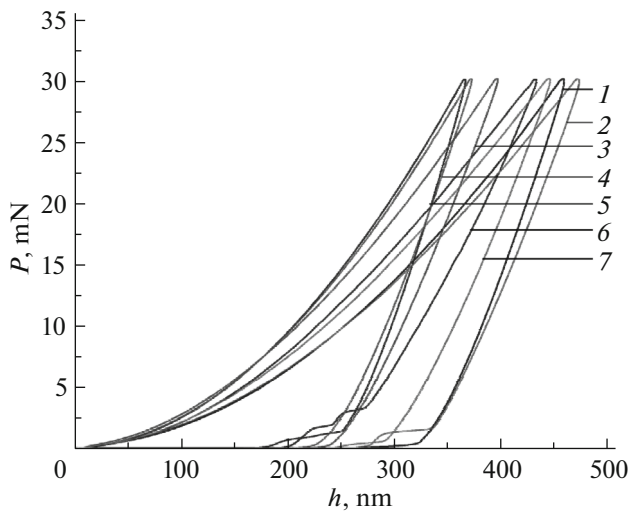
Fig. 7. Diagrams (P–h) of (*1*) the original sample and the samples after thermal treatment at $T = $ (*2*) 300, (*3*) 350, (*4*) 400, (*5*) 550, (*6*) 650, and (*7*) 750°C for 10 min.
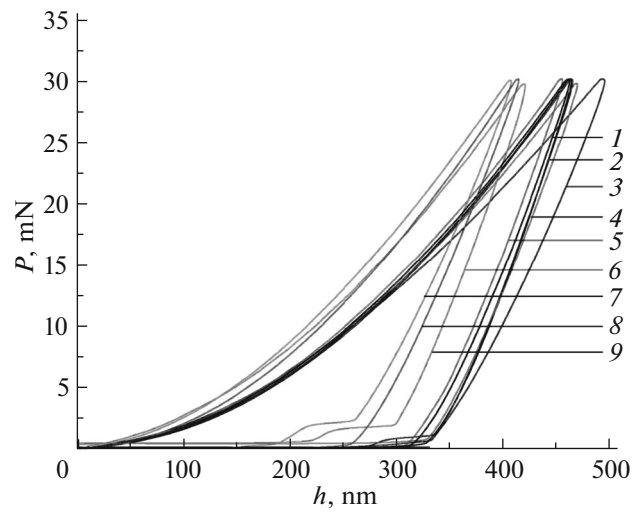
Fig. 8. Diagrams (P–h) of (*1*) the original sample and the samples after photon treatment at the radiation dose received by the sample of $D = $ (*2*) 10, (*3*) 15, (*4*) 20, (*5*) 25, (*6*) 30, (*7*) 35, (*8*) 40, and (*9*) 60 J/cm^2.

These patterns are consistent with the general conclusion of [18] about the loss of plasticity and an increase in the modulus of elasticity. Despite the well-known idea that after full crystallization, the plasticity becomes close to zero, the local plasticity in a completely crystallized sample is comparable to the initial one, that is, an amorphous sample. Considering the structural organization of the Fe$_3$P crystalline phase, this reflects the common plastic deformation mechanism under the action of a concentrated load (nanoindentation): intercluster slippage as an analogue of intergranular slippage (a negative Hall–Petch effect). Slippage occurs because the metal bond (Fe–Fe) is smaller than the covalent bond in the Fe$_3$P tetrahedral cluster. In the Fe–P system, the p^6 shell is excited as a result of the collectivization of phosphorus valence electrons. Their overlap with the $3d^6$ iron shell ensures a strong bond of atoms, which can contribute to the nucleation of structural tetrahedral units during the formation of the amorphous phase, when the kinetics corresponding to a high cooling rate still does not
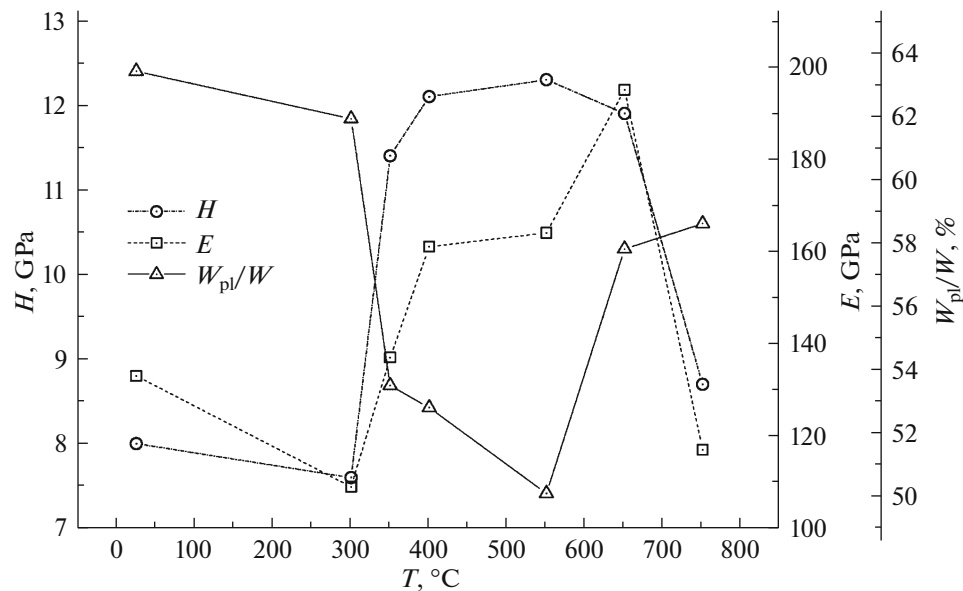

Fig. 9. Hardness, modulus of elasticity, and the proportion of plastic deformation in the work of nanoindentation of the original sample and the samples after thermal treatment at different temperatures.
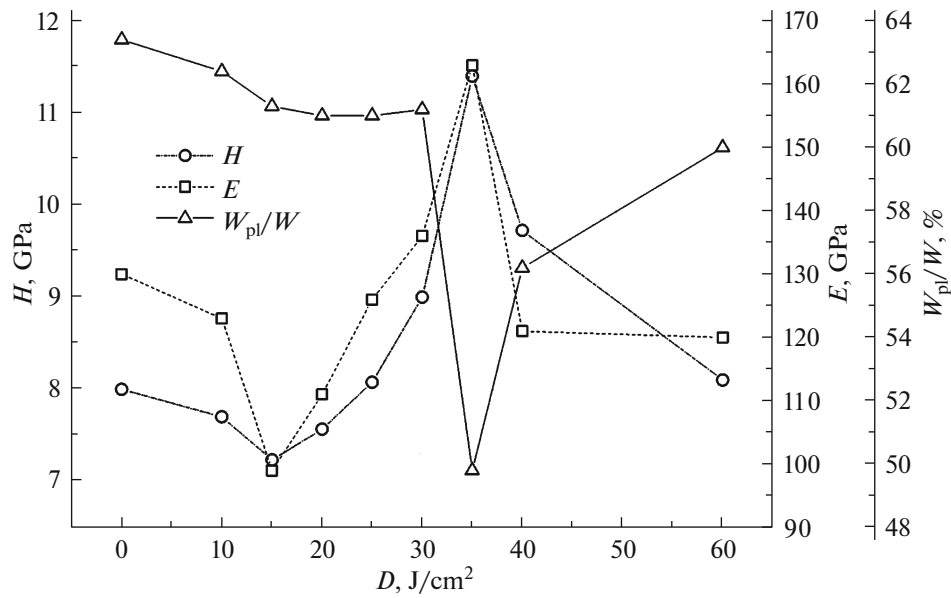
Fig. 10. Hardness, modulus of elasticity, and the proportion of plastic deformation in the work of nanoindentation of the original sample and the samples after photon treatment at different radiation doses.

allow nuclei of the crystalline phase of such a complex structural organization to form.

It follows from Fig. 11 that under uniaxial tension of the amorphous alloy, the deformation has an elastic character. Its value reaches ~1.25% at $\sigma_B = 370$ MPa. A mechanical hysteresis loop under cyclic loading–unloading (Fig. 11, inset) indicates the residual plastic
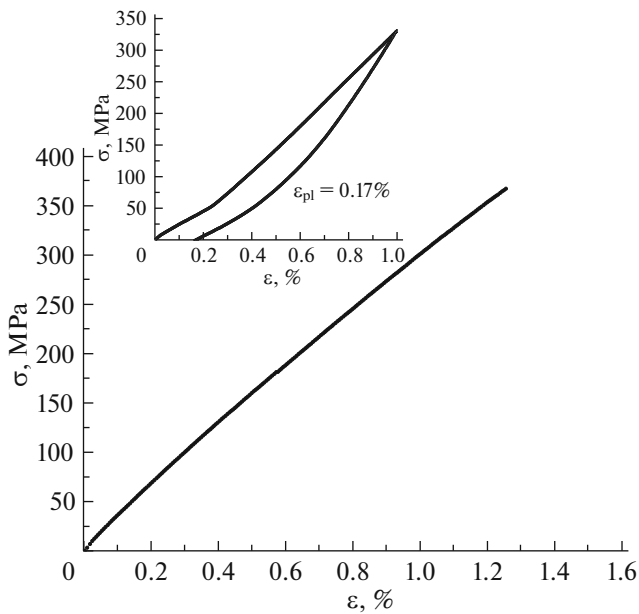

Fig. 11. Stress–strain diagram in tensile tests of the original amorphous alloy. Inset: cyclic tension diagram of the amorphous alloy with the subsequent removal of the load.

deformation of the sample, which at a strain of 1% was 0.17%. Therefore, the low plasticity of the amorphous alloy can reflect the manifestation of microplasticity at each stage of loading as a result of slipping of nucleus clusters of crystalline phases. The elastic deformation of the amorphous alloy confirms mainly the fact that such alloys are characterized only by high local plasticity, as a result of the fundamental difference between the slipping mechanism and the dislocation mechanism implemented in crystalline bodies. Dislocations in crystals move at the speed of sound, which is impossible for cluster movement. Therefore, in contrast to the dislocation mechanism, the cooperative effect of the relay movement of clusters manifests itself in deformation slowly, which is consistent with the ideas about the movement of groups of atoms in the process of deformation of the amorphous alloy [6].

4. CONCLUSIONS

1. With the same sequence of structural changes, the crystallization rate under photon treatment is more than two orders of magnitude higher than that under thermal treatment, which indicates the effect of a high rate of input of the process activation energy.

2. The nonmonotonic dependence of the hardness, elastic modulus, and the proportion of plastic strain in the indentation work is found depending on the annealing temperature or radiation dose received by the sample, as a result of structural changes in the alloy.

3. A conclusion about the cluster mechanism of plastic deformation of the amorphous alloy was formulated based on the features of the crystal structure

of the Fe_3P phase (the impossibility of the dislocation mechanism of plastic deformation) and assuming that the structural unit (tetrahedral Fe_3P cluster) of the crystallized and amorphous alloy is identical.

CONFLICT OF INTEREST

The authors declare that they have no conflict of interest.

REFERENCES

1. C. A. Schuh, T. C. Hufnagel, and U. Ramamurty, Acta Mater. **55**, 4067 (2007).

2. A. S. Argon and H. Y. Kuo, Mater. Sci. Eng. A **39**, 101 (1979).

3. D. Srolovitz, V. Vitek, and T. Egami, Acta Met. **31**, 335 (1983).

4. J. S. Langer, Scr. Mater. **54**, 375 (2005).

5. M. H. Cohen and D. Turnbull, J. Chem. Phys. **31**, 1164 (1959).

6. F. Spaepen, Acta Met. **25**, 407 (1977).

7. A. S. Bakai, *Policluster Amorphous Bodies* (Energoatomizdat, Moscow, 1987) [in Russian].

8. *Institute of Silicate Chemistry of RAS — 80 Years. Historical Essays*, Ed. by V. Ya. Shevchenko (Art-Ekspress, St. Petersburg, 2016) [in Russian].

9. Yu. I. Golovin, *Nanoindentation and its Capabilities* (Mashinostroenie, Moscow, 2009) [in Russian].

10. A. V. Evteev, A. T. Kosilov, and E. V. Levchenko, in *Proceedings of the Conference on Amorphous Precision Alloys* (Moscow, 2000), p. 62.

11. V. M. Ievlev, A. V. Kostyuchenko, B. M. Darinskii, and S. M. Barinov, Phys. Solid State **56**, 321 (2014).

12. V. M. Ievlev, S. M. Barinov, V. S. Komlev, A. Y. Fedotov, and A. V. Kostyuchenko, Ceram. Int. **41**, 10526 (2015).

13. https://materials.springer.com/isp/crystallographic/docs/sd_0452183.

14. S. Huang, *Structure and Structure Analysis of Amorphous Materials* (Clarendon, Oxford, 1984).

15. G. E. Abrosimova, A. S. Aronin, and N. N. Kholstin, Phys. Solid State **52**, 445 (2010).

16. W. C. Oliver and G. M. Pharr, J. Mater. Res. **7**, 1564 (1992).

17. M. C. Antonova, E. K. Belonogov, A. V. Boryak, V. V. Vavilova, V. M. Ievlev, S. V. Kannykin, and N. A. Palii, Inorg. Mater. **51**, 283 (2015).

18. A. M. Glezer, *Melt-Hardened Nanocrystals* (Fizmatlit, Moscow, 2012) [in Russian].

Translated by O. Zhukova